JOURNAL OF Materials CHEMISTRY

Lithium insertion in two tetragonal tungsten bronze type phases, $M_8W_9O_{47}$ (M = Nb and Ta)

Sagrario M. Montemayor, A. Alvarez Mendez, A. Martínez-de la Cruz, Antonio F. Fuentes* and Leticia M. Torres-Martínez

Facultad de Ciencias Químicas, División de Estudios Superiores, Universidad Autónoma de Nuevo León, Apartado Postal 1625, Monterrey, Nuevo León, Mexico. E-mail: afernand@ccr.dsi.uanl.mx

Received 10th June 1998, Accepted 21st September 1998

A study of lithium insertion in two tetragonal tungsten bronze (TTB) type phases of general formula $M_8W_9O_{47}$ (M = Nb and Ta), is presented. The electrochemical insertion of up to 20 lithium atoms per formula unit in $Nb_8W_9O_{47}$ ($Li/\Sigma M = 1.2$) proceeds through a reversible reaction with several single phase and one two-phase domains, while in $Ta_8W_9O_{47}$ the reversibility of lithium insertion is limited to 15 atoms ($Li/\Sigma M = 0.9$). Structural changes on $Nb_8W_9O_{47}$ as a function of the number of lithium atoms inserted have been studied by X-ray powder diffraction.

Introduction

The study of the chemistry of tungsten bronzes and related phases has attracted considerable attention because of their potential use as electrodes, catalysts and in optical displays. Additionally, these phases were found to present interesting optical and ferroelectric properties. In this context and continuing with work started recently in our research group on insertion reactions in some niobium–tungsten mixed oxides,[1–3] a study of lithium insertion in two tetragonal tungsten bronze (TTB) type phases of general formula $M_8W_9O_{47}$ (M = Nb and Ta), has been carried out.

From the solid state chemistry point of view, the Nb_2O_5–WO_3 and Ta_2O_5–WO_3 systems behave in a fairly similar way in the region rich in WO_3. Phases containing between 50 and 80 wt.% of WO_3, present a structure similar to the so-called *tetragonal tungsten bronzes* (TTB). These phases consist in a framework of MO_6 octahedra sharing corners, linked in such a way that three, four- and five-sided tunnels are formed. Decreasing oxygen-to-transition metal ratio (3 in WO_3 *vs.* 2.76 in $M_8W_9O_{47}$) is achieved in these TTB type phases by filling a certain number of five-sided tunnels with oxygen and metal atoms thus forming the so-called pentagonal columns (PCs for short):[4] a MO_7 pentagonal bipyramid sharing equatorial edges with five MO_6 octahedra. In $Nb_8W_9O_{47}$ (Fig. 1) one third of the pentagonal tunnels are occupied in this way.[5–7] Cation sites with pentagonal bipyramidal coordination are preferentially occupied by niobium while in the corner sharing metal–oxygen octahedra, metal atoms are on average (0.4 Nb + 0.6 W).

While only one polymorph for $Nb_8W_9O_{47}$ has been reported to exist, two have been found for $Ta_8W_9O_{47}$, a low (tetragonal) and a high temperature form (orthorhombic), both exhibiting TTB type structures, although only in the high temperature one (1400 °C) is it possible to observe threefold TTB-type superstructure.[8] A similar cation distribution to that found for the niobium–tungsten mixed phases was also proposed here. It is important to point out that although $M_8W_9O_{47}$ is the ideal composition, a small range of non-stoichiometry may exist in both niobium and tantalum TTB type phases, due to disorder in the tunnels occupancy.

Compounds presenting structures containing PCs as main building units, such as $W_{18}O_{49}$, have been already studied as host materials for reversible lithium insertion reactions.[9] In this work a study of the electrochemical lithium insertion in $M_8W_9O_{47}$ has been carried out. In order to evaluate the influence of lithium insertion on the structure of the parent oxide, some lithiated phases were synthesised by indirect chemical reaction and characterised by X-ray powder diffraction experiments. As the main difference between both mixed tungsten oxides is the presence of Nb^{5+} instead of Ta^{5+}, it would be interesting to compare their behaviour *versus* lithium insertion reactions. No attempt is made in this work on testing $M_8W_9O_{47}$ as cathode materials in lithium ion batteries.

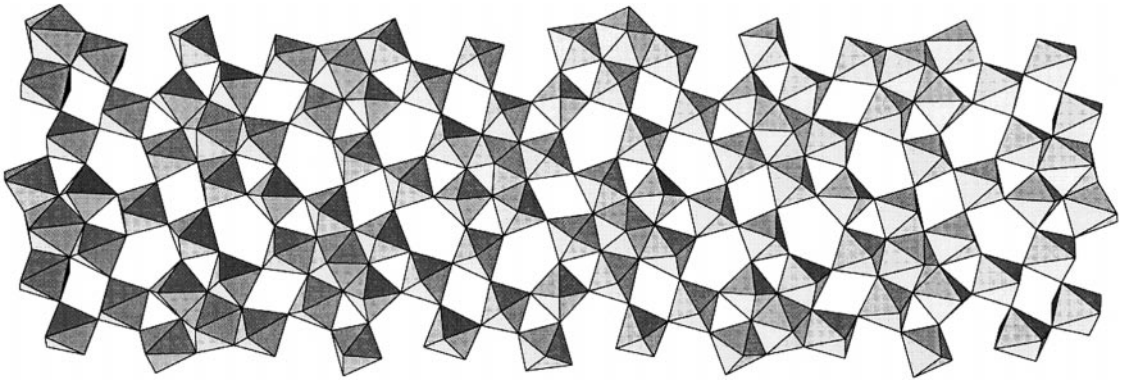

Fig. 1 Idealised structure of $Nb_8W_9O_{47}$. When joining the different polyhedra, five-, four- and three-sided tunnels are formed where additional ions can be inserted.

Experimental

Preparation and characterisation of pristine materials, $M_8W_9O_{47}$

The tantalum–tungsten and niobium–tungsten mixed oxides used in this study were synthesised by solid state reaction. The starting materials, WO_3 (Aldrich Chem. Co, 99+%), Nb_2O_5 (Alfa Products 99.5%) and Ta_2O_5 (Aldrich Chem. Co, 99.99%), were weighed in the appropriate stoichiometric ratio (4 M_2O_5 : 9 WO_3) and thoroughly mixed by grinding in an agate mortar using Analar grade acetone. Powders were then pressed into 10 mm diameter pellets, placed in a platinum crucible and fired at 1250 °C in an electrical furnace. During firing samples were periodically extracted from the furnace and ground to favour reaction before being finally quenched at room temperature. Phase identification was carried out by X-ray powder diffraction in a Siemens D-5000 diffractometer using Cu-Kα radiation ($\lambda = 1.5418$ Å). A typical diffraction experiment for determining cell parameters was run with a step size of 0.12° min^{-1} using KCl as internal standard.

Electrochemical lithium insertion

Electrochemical experiments were carried out with a multichannel potentiostatic-galvanostatic system MacPile II,[10] using a Swagelok™ type cell[11] with metal lithium acting simultaneously as negative and reference electrode. Positive electrodes were prepared by mixing the phase being tested, $Nb_8W_9O_{47}$ or $Ta_8W_9O_{47}$, with carbon black and a binder, (0.5% ethylene–propylene–diene terpolymer, EPDT, in cyclohexane) either in a 89 : 10 : 1 ratio (wt.%) for niobium containing samples or in a 59 : 40 : 1 ratio for the tantalum compound (this material is not a good electronic conductor so a larger proportion of carbon has to be used). The electrolyte used was a 1 mol dm^{-3} solution of $LiClO_4$ in a previously dried 50 : 50 mixture of ethylene carbonate (EC) and diethoxyethane (DEE). Cell assemblage was carried out in a MBraun glove box under an argon atmosphere with continuous purge of water vapour and oxygen ensuring an inside concentration for both compounds of <1.5 ppm.

Two different electrochemical experiments were carried out on these cells, either in a current or in a potential-controlled mode. Potentiodynamic titrations were carried out by a stepwise technique also known as step potential electrochemical spectroscopy, SPECS.[12] In this technique, the potential is stepwise increased or decreased while recording charge increments *vs.* time at each potential level and therefore allowing the study of insertion reaction kinetics. The simultaneous determination of incremental capacities and observation of the kinetics of the redox process helps in determining the succession of single phase and two phase domains which might take place on insertion/deinsertion. Typical experimental conditions were set at ± 10 mV (2 h)$^{-1}$ potential steps with a charge recording resolution of 5 μA h and a strict temperature control.

Lithium chemical insertion

Lithium insertion was also carried out by chemical reaction of $Nb_8W_9O_{47}$ with an appropriate reducing agent, *n*-butyllithium in *n*-hexane. A given volume of this reagent (1.6 mol dm^{-3}) was added to a known weight of host material previously placed in a glass reaction vessel. The mixture was stirred for 7 days. Reaction products were thoroughly washed with *n*-hexane, dried and stored in the glove box. Lithium content in $Li_xNb_8W_9O_{47}$ was analysed by AAS using a Varian SpectrAA5 spectrometer after extraction of the inserted ions using concentrated nitric acid. Phase identification was carried out by X-ray powder diffraction as described above. Although lithium inserted $Nb_8W_9O_{47}$ proved to be stable at least during the time of observation, intercalated samples were covered by a polyethylene film while recording data on the diffractometer to prevent sample oxidation.

Results and discussion

Electrochemical lithium insertion in $Nb_8W_9O_{47}$

Electrochemical lithium insertion in $Nb_8W_9O_{47}$ was carried out by discharging a cell with the following configuration:

$$Li|1\ mol\ dm^{-3}\ LiClO_4\ in\ (50\%\ DEE + 50\%\ EC)|Nb_8W_9O_{47}$$

Results obtained from SPECS experiments run down to 1.1 V *vs.* Li^+/Li using ± 10 mV (2 h)$^{-1}$ potential steps, are shown in Fig. 2 as an *E vs.* composition (*x* in $Li_xNb_8W_9O_{47}$) plot. As can be seen in this graph, $Nb_8W_9O_{47}$ can reversibly incorporate up to 20 lithium atoms per formula unit which correspond to about 1.2 Li per metal atom. Almost all lithium atoms inserted are removed after completing a charge–discharge cycle. The main features of this plot are two plateaux, A and B, of approximately constant *E* values around 2.1 and 1.7 V *vs.* Li^+/Li separating three regions where a continuous variation of *E* with composition is observed. In order to determine the existence of continuous transformations or to multiphase regions, potentiostatic experiments were analysed in more detail. Representing these results as $\Delta Q/m$ *vs.* *E*, Fig. 3, it is possible to see that the electrochemical lithium insertion in this material goes really through three very well defined reduction steps labelled here as A, B and C. The electrochemical lithium extraction from $Li_xNb_8W_9O_{47}$ follows a similar mechanism and three analogous steps, labelled as A′, B′ and C′, are also present.

It was observed that the nature of the first step (labelled as A and A′) was always better defined on oxidation and second

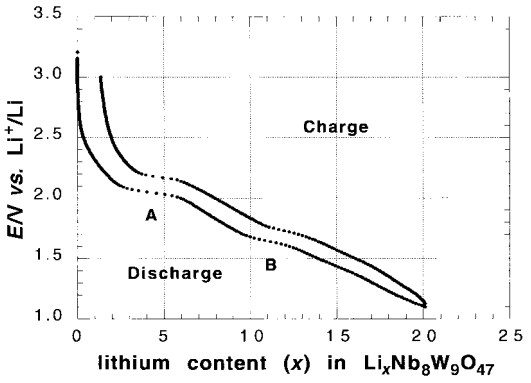

Fig. 2 Evolution of cell voltage *versus* composition (*x* in $Li_xNb_8W_9O_{47}$) obtained during a SPECS experiment run at ± 10 mV (2 h)$^{-1}$ potential steps showing a complete charge–discharge cycle.

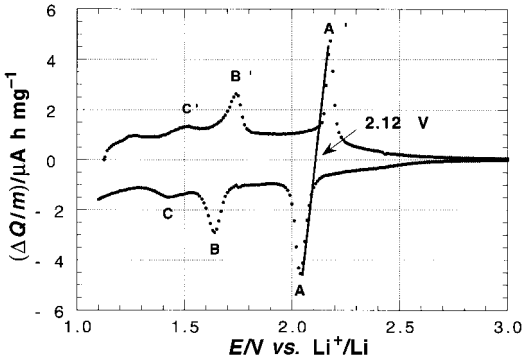

Fig. 3 $\Delta Q/m$ *vs.* *E* plot obtained from a SPECS experiment run at ± 10 mV (2 h)$^{-1}$ potential steps showing the different reduction and oxidation steps observed on lithium insertion and extraction.

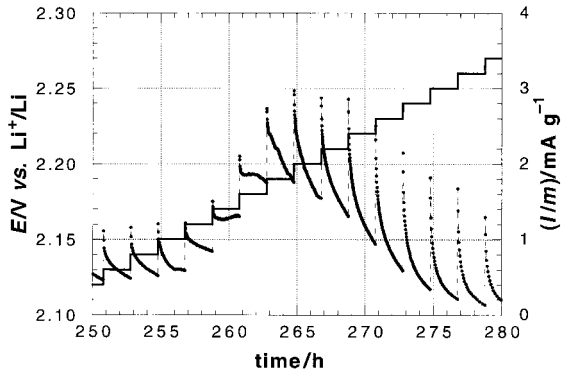

Fig. 4 Evolution of cell current (·····) and voltage (———) with time during a SPECS experiment run using $+10$ mV $(2\text{ h})^{-1}$ potential steps.

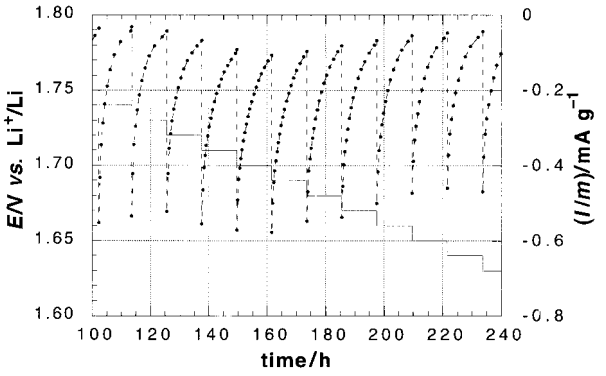

Fig. 6 I/m and E *vs.* time plot obtained when crossing at -10 mV $(12\text{ h})^{-1}$ potential steps the voltage region where peak B was observed.

reduction than on the first discharge. Therefore, we shall start examining a chronoamperogram obtained when crossing at $+10$ mV $(2\text{ h})^{-1}$ potential steps, the potential region where the oxidation peak A′ was observed, Fig. 4. The I *vs.* time plot shows a profile obviously not governed by a simple diffusion process which would give a monotonic tendency towards $I=0$, but it is typical of a first order transition. In this type of process, the response to a potential step will depend on the mobility of the interface between the two phases, relative to lithium diffusivity in both phases and on the kinetics of lithium transfer at the interface with the electrolyte assuming that there is no electronic conductivity limitation.[13] Thus, it could be assumed that the first reduction step A which corresponds to the first plateaux (at higher E values) also labelled as A in Fig. 2, can be associated with a multiphase domain separating two solid solution regions, I and II. The phase I–phase II equilibrium potential can be given as the intercept at the slope extrapolations at zero current, *i.e.* 2.12 V. Fig. 5 shows the evolution of the cell voltage *versus* composition obtained when cycling a similar cell to the one described elsewhere in this work, between 3 and 1.75 V *vs.* Li^+/Li. As can be seen in this graph, phase I transformation to phase II is a reversible process with all the atoms initially incorporated being extracted after completing a charge–discharge cycle. Since potentiostatic experiments run at ±10 mV $(2\text{ h})^{-1}$ potential steps did not reveal unambiguously the exact nature of reduction steps labelled in Fig. 3 as B and C and their corresponding oxidation steps B′ and C′, it was necessary to run experiments at much lower scan rates [±10 mV $(12\text{ h})^{-1}$]. Time dependence of the current when crossing at -10 mV $(12\text{ h})^{-1}$ potential steps, the voltage region where the reduction peak labelled in Fig. 3 as B was found, is shown in Fig. 6. In this case, the monotonic tendency towards $I=0$ observed in the current decay *vs.* time plot, can be associated with a continuous transformation. In homogeneous solutions and assuming that there is no ion–ion interaction, the system behaves in a similar way independently of the amount of lithium atoms inserted.[14] A similar behaviour of the current decay *versus* time is observed on the third reduction peak labelled in Fig. 3 as C making for a second continuous transformation between 1.3 and 1.6 V *vs.* Li^+/Li on lithium insertion in $Nb_8W_9O_{47}$.

A confirmation of these observations is presented in Fig. 7 which shows a comparison between two voltamperograms obtained when running SPECS experiments ±10 mV $(2\text{ h})^{-1}$ (filled circles) and ±10 mV $(12\text{ h})^{-1}$ (open squares) potential steps. While steps labelled as A and A′ show hysteresis in both experiments (initial slopes can be aligned) independently of the voltage scanning rate used, confirming our previous assumption of dealing with a first order phase transition at this potential range, a different situation is observed for steps labelled B and C. In these latter cases and for the experiment run at ±10 mV $(12\text{ h})^{-1}$, hardly any hysteresis effect is noticed between reduction and oxidation peaks. On the contrary, peaks B′ and C′ are now found located on top of peaks B and C supporting the idea of crossing two consecutive continuous phase transitions between 1.8 and 1.3 V *vs.* Li^+/Li. Therefore, a complete phase diagram $Li–Nb_8W_9O_{47}$ can be now proposed as follows: above 2.12 V *vs.* Li^+/Li, a solid solution domain (I) from $x=0$ to $x\approx2$. At 2.12 V *vs.* Li^+/Li, a two phase equilibrium between phase I and phase II. Below 2.12 V *vs.* Li^+/Li, a solid solution domain (II) from $x=6$. Around 1.7 V *vs.* Li^+/Li, an incremental capacity peak probably due to a tendency to local ordering in phase II around $11<x<12$. Below 1.7 V *vs.* Li^+/Li, continuation of phase II with another possible tendency to local ordering giving rise to an increase of the incremental capacity of the cell around 1.4–1.5 V *vs.* Li^+/Li.

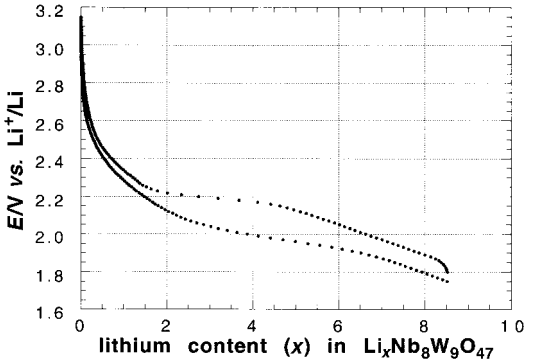

Fig. 5 E (V *vs.* Li^+/Li) *vs.* lithium content (x) in $Li_xNb_8W_9O_{47}$ plot obtained when cycling a cell within a limited potential window.

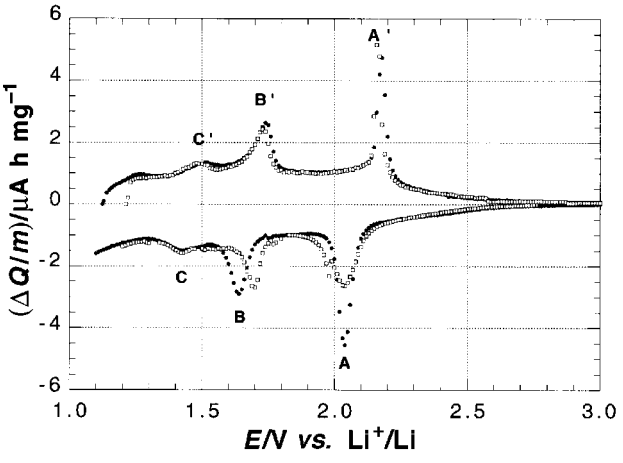

Fig. 7 Comparison between two $\Delta Q/m$ *vs.* E plots obtained when running SPECS experiments at ±10 mV $(2\text{ h})^{-1}$ and ±10 mV $(12\text{ h})^{-1}$ potential steps.

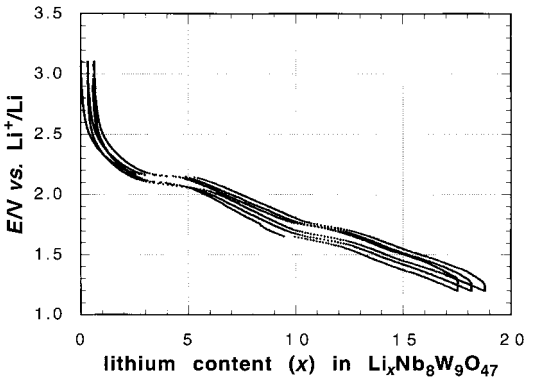

Fig. 8 *E vs.* lithium content (x) in $Li_xNb_8W_9O_{47}$ plot obtained after completing three charge–discharge cycles.

Lithium insertion reaction reversibility in this material can be better appreciated in Fig. 8 where results obtained after completing three charge–discharge cycles in a cell configured as mentioned above are presented. Cycling is carried out with minimal capacity losses. Data shown were obtained from a galvanostatic experiment run at a cycling rate greater than C/76 (C/76 corresponds to a charge or a discharge within 76 h).

According to the structure shown in Fig. 1, a total of 26 different tunnels are found in a unit cell of this phase which will also contain two formula units of $Nb_8W_9O_{47}$. These cavities are distributed as follows: 8 five-sided tunnels; 6 four-sided and 12 three-sided channels. In order to be able to accommodate 40 lithium atoms (20 per formula unit) in 26 tunnels of a unit cell, multiple lithium occupancy has to be assumed in some cavities (ratio of lithium atoms intercalated in a unit cell to available cavities $=1.54$). Based on tunnel size, it is most likely that only one lithium atom would enter into three-sided tunnels. This assumption would leave 28 lithium atoms to be distributed in 14 tunnels which makes a lithium atoms to available cavities ratio of 2. Thus, It is reasonable to suggest that two lithium atoms would enter in each of the four (coordination number 12) and five-sided tunnels (coordination number 15). With the available data it is not possible to give a filling sequence of these cavities.

Electrochemical lithium insertion in $Ta_8W_9O_{47}$

A preliminary study of the electrochemical lithium insertion in $Ta_8W_9O_{47}$, an isostructural phase with $Nb_8W_9O_{47}$ containing tantalum instead of niobium, was carried out by discharging a similar cell to the one described above. Results obtained from a SPECS experiment run at ± 10 mV $(2\ h)^{-1}$ potential steps, are shown in Fig. 9 as the evolution of cell voltage *versus* composition (x in $Li_xTa_8W_9O_{47}$). Only slight slope changes are observed with apparently no existence of voltage

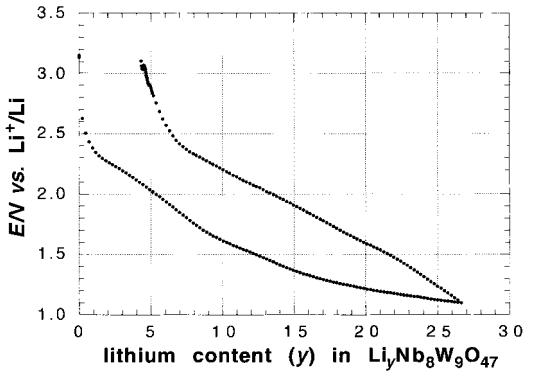

Fig. 9 Evolution of cell voltage *vs.* composition (x in $Li_xTa_8W_9O_{47}$) obtained during a SPECS experiment run at ± 10 mV $(2\ h)^{-1}$ potential steps showing a complete charge–discharge cycle.

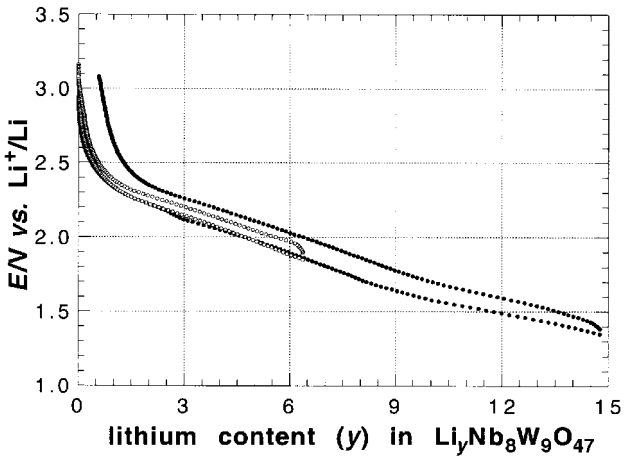

Fig. 10 *E vs.* lithium content (x) in $Li_xTa_8W_9O_{47}$ plot obtained from a SPECS experiment run at ± 10 mV $(2\ h)^{-1}$ potential steps showing two complete charge–discharge cycles within limited potential windows.

plateaux indicating multiphase regions. As can be seen in this plot, $Ta_8W_9O_{47}$ incorporates a larger number of lithium atoms per formula unit (27, $Li/\Sigma M = 1.6$) than its niobium analogue (20 Li/formula unit) between 3.1 and 1.1 V. However, almost 17% of those atoms remained in the structure after completing a charge–discharge cycle showing therefore the existence of larger structural changes on insertion. Fig. 10 shows the evolution of the cell voltage *versus* composition for a similar cell to the one described above but cycled up to 1.85 (open dots) and 1.35 volts (solid dots) showing this time that the insertion of up to 15 lithium atoms in $Ta_8W_9O_{47}$ ($Li/\Sigma M = 0.9$), is a reversible reaction.

Both ions Nb^{5+} and Ta^{5+} have similar ionic radii (0.64 Å, six-coordinate),[15] but contain a different number of electrons (36 and 68 respectively). Therefore, Ta^{5+} has a larger electronic density than Nb^{5+} which makes lithium diffusion more difficult in $Ta_8W_9O_{47}$ relative to that in $Nb_8W_9O_{47}$ and proving that these metals play an important role in the insertion reaction. An attempt was made to prepare lithiated phases by chemical reaction with *n*-butyllithium but these proved to be extremely unstable upon exposure to the atmosphere.

Chemical lithium insertion in $Nb_8W_9O_{47}$

In order to study the influence of lithium insertion on the structure of the parent oxide, different inserted compositions included in the solid solution regions detected during the electrochemical study, were prepared by chemical reaction of $Nb_8W_9O_{47}$ and *n*-butyllithium. Inserted materials prepared were characterised as previously described and resulted in the following compositions: $Li_{1.8}Nb_8W_9O_{47}$, $Li_{7.3}Nb_8W_9O_{47}$ and $Li_{18.8}Nb_8W_9O_{47}$. Phase characterisation was carried out by X-ray powder diffraction using KCl as internal standard. Powder patterns, which are shown in Fig. 11, were indexed using the same orthorhombic cell described in the literature for the starting material by using a least-squares cell refinement program. Results are shown in Table 1.

Powder patterns showed a gradual change in position and intensity of some reflections as the insertion reaction proceeded which can be related with small displacements of the atoms in $Nb_8W_9O_{47}$ in order to accommodate the lithium ions. The most important changes are observed between diffraction patterns b and c which correspond to phase I transition to phase II. A colour change for these materials was observed as the number of lithium atoms incorporated increased, going from pale yellow for the pristine phase to blue developing to black for phase II which corresponds to an increase in the electronic conductivity of $Nb_8W_9O_{47}$ as the insertion reaction

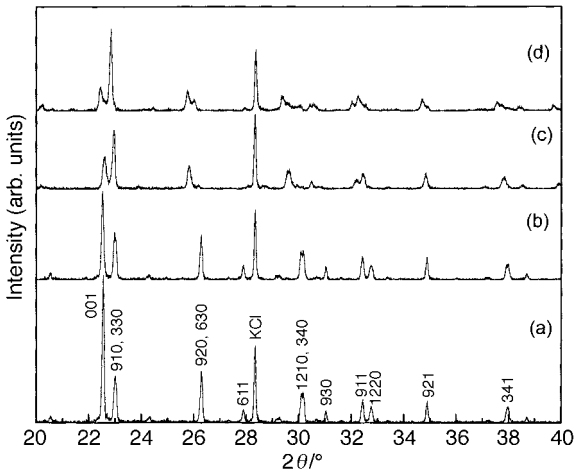

Fig. 11 X-Ray powder diffraction patterns of (a) $Nb_8W_9O_{47}$, (b) $Li_{1.8}Nb_8W_9O_{47}$, (c) $Li_{7.3}Nb_8W_9O_{47}$ and (d) $Li_{18.8}Nb_8W_9O_{47}$.

Table 1 Cell parameters and cell volume values obtained from X-ray powder diffraction data for $Li_xNb_8W_9O_{47}$

Compound	a/Å	b/Å	c/Å	Cell volume/Å^3
$W_9Nb_8O_{47}$[a]	36.692	12.191	3.945	1764.65
$W_9Nb_8O_{47}$	36.675(8)	12.186(2)	3.9447(8)	1763.0±0.7
$Li_{1.8}Nb_8W_9O_{47}$	36.71(1)	12.201(4)	3.942(1)	1766.1±0.9
$Li_{7.3}Nb_8W_9O_{47}$	36.9(1)	12.29(3)	3.93(1)	1787.8±9.0
$Li_{18.8}Nb_8W_9O_{47}$	36.9(1)	12.28(5)	3.94(1)	1790.0±12.7

[a]Ref. 5.

proceeds. Powder patterns obtained after Li removal were very similar to those of the pristine phase confirming the reversibility of this reaction.

Conclusions

A study of lithium insertion in $M_8W_9O_{47}$ (M = Nb and Ta), a tetragonal tungsten bronze type phase (TTB) has been carried out. The electrochemical insertion of up to 20 lithium atoms per formula unit of $Nb_8W_9O_{47}$ (Li/ΣM = 1.2) is a reversible reaction which proceeds through three reduction steps: a first order transition at around 2.12 V and two continuous transformations at around 1.70 and between 1.40 and 1.50 V *vs.* Li^+/Li. These transformations originated at least two solid solution regions of general formula $Li_xNb_8W_9O_{47}$ with the following approximate composition limits: I: $0 \leqslant x \leqslant 2$; II: $6 \leqslant x \leqslant 20$. Two incremental capacity peaks observed at 1.70 V ($11 < x < 12$) and between 1.40 and 1.50 V probably indicate the existence of a tendency to local ordering in phase II. These results are supported by X-ray diffraction data of inserted materials which show important changes on the transition from phase I to II with additional variations as the number of lithium atoms inserted increased. In order to accommodate such a number of lithium atoms and taking into account the number of tunnels available per unit cell, multiple lithium occupancy has to be considered in some cavities.

Electrochemical lithium insertion was also studied in $Ta_8W_9O_{47}$ where the reaction seems to follow a different mechanism confirming that the second transition metal in these TTB type structures (Nb and Ta) plays an important role in the insertion reaction. Lithium insertion reversibility in $Ta_8W_9O_{47}$ was observed for a smaller number of atoms than its niobium analogue (Li/ΣM = 0.9).

Acknowledgements

Financial support from CONACYT (Project 3862P-A9607) is gratefully acknowledged. The authors are also especially grateful to Dr. Yves Chabre for useful discussions and his critical remarks on the original manuscript.

References

1 A. F. Fuentes, A. Martínez de la Cruz and L. M. Torres-Martinez, *Solid State Ionics*, 1996, **92**, 103.
2 A. F. Fuentes, E. Briones Garza, A. Martínez de la Cruz and L. M. Torres-Martínez, *Solid State Ionics,* 1997, **93**, 245.
3 A. F. Fuentes, A. Martínez de la Cruz and L. M. Torres-Martinez, *Mater. Res. Soc. Symp. Proc*., 1997, **453**, 659.
4 M. Lundberg, *Chem. Commun. Univ. Stockholm*, 1971, No. XII.
5 R. S. Roth and J. L. Waring, *J. Res. Nat. Bur. Stand.*, *Sect. A*, 1966, **70**, 281.
6 A. W. Sleight, *Acta Chem. Scand.*, 1966, **20**, 1102.
7 D. C. Craig and N. C. Stephenson, *Acta Crystallogr.*, *Sect. B*, 1969, **25**, 2071.
8 F. Krumeich and T. Geipel, *J. Solid State Chem.,* 1996, **124**, 58.
9 A. Martínez de la Cruz, F. García-Alvarado, E. Morán, M. A. Alario-Franco and L. M. Torres-Martínez, *J. Mater. Chem.,* 1995, **5**, 513.
10 C. Mouget and Y. Chabre, *Multichannel Potentiostatic and Galvanostatic System MacPile*, Licensed from CNRS and UJF Grenoble to Bio-Logic Corp., 1 Av. de l'Europe, F-38640, Claix, France.
11 J. M. Tarascon, *J. Electrochem. Soc.*, 1985, **132**, 2089.
12 Y. Chabre, *J. Electrochem. Soc.*, 1991, **138**, 329.
13 Y. Chabre and J. Pannetier, *Prog. Solid State Chem.*, 1995, **23**, 1.
14 C. J. Wen, B. A. Boukamp, R. A. Huggins and W. J. Weppner, *J. Electrochem. Soc.*, 1979, **126**, 2258.
15 R. D. Shannon, *Acta Crystallogr.*, *Sect. A*, 1976, **32**, 751.

Paper 8/04410D